Effect of Atmospheric Conditions on Ultraviolet Photoconductivity of Zinc Oxide Nanoparticles

[1]Mohammed A. Ibrahem*, [2]Emanuele Verrelli, [3]Khue T. Lai, [2]Fei Cheng, [4]Mary O'Neill

[1]Laser Science and Technology Branch, Department of Applied Sciences, University of Technology – Iraq

[2]Department of Physics and Mathematics, University of Hull – United Kingdom

[3]Department of Engineering and Computer Science, University of Hull – United Kingdom

[4]School of Science and Technology, Nottingham Trent University – United Kingdom

Abstract

ZnO nanoparticles have gained considerable interest lately due to their remarkable optical and electrical properties, which enable them to have the potential to be the next generation of transparent semiconductors. However, interactions with atmospheric water and surface carbonates limited and seriously threatened device stability and dependability. The UV photoconductivity of the ZnO NP films is heavily influenced by oxygen adsorption and organic species in the ambient air. The stability of the ZnO photodetector prepared, annealed, and tested in a nitrogen atmosphere was improved in terms of current magnitude and sustaining photocurrent cycles. ZnO NPs films processed in the air show considerable change in surface composition compared to nitrogen indicated by surface organic complexes. In an oxidized manufacturing environment, the compounds above were effectively eliminated while partly degraded in nitrogen. We find that the ZnO NPs surface is highly reactive with ambient CO_2, generating surface carbonates groups that promote electrically active surface states.

1. Introduction

ZnO nanoparticles (NPs) have attracted substantial attention in electronic and optoelectronic devices due to their superb properties, which enable them to be the semiconductor of choice in solution-processed thin film technology such as in thin film transistors (TFTs) and UV photodetectors [1],[2],[3],[4]. The importance of UV photodetection is highly appreciated in various applications such as in the military, aerospace, and biology [5]. These applications often require a reliable measurement positively linked with device stability [6]. Solution-processed photodetectors have multiple challenges, including grain size and boundaries and the added organic ligands, which affect the device performance by limiting electron transportation. Long-term device stability in ambient conditions has always been a significant issue that impacts the applicability of solution-processed UV photodetectors and TFT devices [7], especially those involving ZnO nanostructures. ZnO shows tremendous advantages, such as superb UV photoconductivity, due to its wide optical bandgap of 3.37 eV at room temperature, low production cost, and high environmental tolerance. However, ZnO-based photodetectors are

still not commercialized because of their photoresponse sensitivity to ambient conditions such as oxygen, humidity, and other organic-based substances. The photoresponse of ZnO is well documented in the literature with its electronic redistribution dependency on surface oxygen absorption\desorption processes in the dark and in the UV, respectively [8]. Electron-hole pairs are photogenerated when UV light is irradiated. The holes migrate to the ZnO surface via the potential gradient caused by band bending in the energy levels, desorbing oxygen molecules from the surface, and releasing trapped electrons into the conduction band. The photoabsorption process generates electrons in addition to those released from the surface area, significantly increasing the ZnO conductivity upon irradiation with UV light [9]. Photoconductivity of ZnO has also been examined in the vacuum, with photocurrent continuing to grow at low oxygen pressure, corroborating the role of oxygen adsorption [8],[10]. Thomas et al. [11] suggested that eliminating adsorbed oxygen from the surface of ZnO might not be the reason for the rise in photoconductivity in a vacuum. Bao et al. [12], who similarly ascribed the large photocurrent in vacuum to the photodecomposition of ZnO under UV irradiation, support the abovementioned theory. Gurwitz et al. [13] suggested that ZnO lattice decomposition is also taking place due to the photo-reduction of ZnO by environmental carbon molecules adsorbed on the surface. This observation is consistent with our recent findings on the involvement of adsorbed carbon in the visible photoconductivity of ZnO [14]. Water is another essential factor that exists naturally in an atmospheric condition which is also found to play a critical role in affecting ZnO photoresponse and recovery speed by a competitive adsorption process with oxygen molecules on the oxygen vacancies sites. The adsorption speed is faster for water molecules than oxygen, which accelerates the photoconductivity recovery speed. Atmospheric dissociation of water molecules on the vacancy sites generates hydroxyl groups by hydroxylating a vacancy neighboring the lattice oxygen (O_o) which captures free electrons and therefore reduces the ZnO conductivity: $H_2O + O_o + 2e- \rightarrow 2OH^-$ [15]. However, with more water adsorbed on the surface, a condensed water layer starts to form, ionizing the surface and leading to proton conductivity (H^+) according to Grotthuss mechanism: $2H_2O \rightarrow H_3O + OH^-$ [16]. This process is significantly increasing the conductivity. An observation by Greenham et al. [17] suggested that oxygen adsorption mainly affects charge injection rather than bulk transport traps on the surface. In other words, oxygen re-adsorbed on the Schottky junction interfacing the electrode and the ZnO plays the leading role in the fast dropping of the current after switching off the light source when the device is tested in the air. ZnO photostability is critical, nevertheless, it is not yet fully comprehended due to the absence of consensus about ZnO UV photo-mechanism. The oxygen molecules adsorption on the surface of ZnO NPs from the ambient environment is thought to affect the UV photoresponse of ZnO. According to this study, the magnitude and temporal dependency of ZnO UV photoconductivity can be influenced by device preparation, storage, and measurement conditions. We aim to demonstrate that various surface species, such as water and/or surface carbonates, are equally important and affect the UV photoconductivity of ZnO NPs.

2. Experimental Procedure

ZnO nanoparticles suspension with a concentration of 2.5 % by weight dissolved in chloroform formed the active layer in planar configuration UV photodetector devices. The suspension preparation and device characterization procedures are similar to those mentioned in our earlier publication [14],[18]. ZnO NPs film was deposited in the air or nitrogen on interdigitated ITO substrates purchased from Ossila, with a film thickness of 120 nm at a fixed spinning speed of 2000 rpm at 30 sec and baking temperature of 100 ℃ for 10 min for device comparability. The utilized ITO fingers (20 Ω/square) have dimensions of 30 mm × 50 μm. ZnO NPs film was annealed at 350 ℃ in air or nitrogen after spin coating and baking to improve film uniformity and eliminate the capping octylamine ligands. There was no vacuum evaporation or severe processing stages in the photodetector production process. Figure 1 shows a schematic illustration of the ZnO UV photodetector configuration. The surface topography of ZnO NPs films after processing in different environments was investigated using atomic force microscopy (AFM) in the tapping mode from Bruker. The surface roughness of AFM images was analyzed using Gwyddion (version 2.47). A Xenon lamp, a 150-W source connected to a monochromator with a 5 nm bandwidth resolution and a set of lenses provides a rectangle-shaped light beam spanning the active device area. BenWin$^+$ software was used to connect the monochromator and the Keithley 2400 to the computer and acquire the photocurrent and transient current at different wavelengths. The photocurrent characteristics were recorded in both air and nitrogen-filled glovebox conditions. FTIR spectra of ZnO samples processed at other conditions, deposited on GaAs substrate, were studied using a Bruker IFS 66/S FTIR spectrometer with 4 cm^{-1} resolution, and 1000 scans were taken and then averaged for each spectrum.
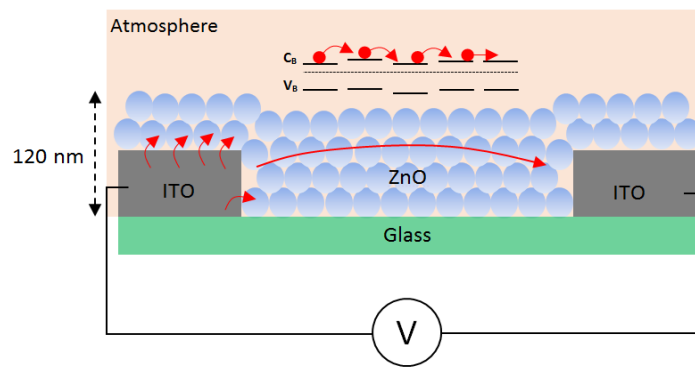
Figure 1: A two-dimensional schematic of the solution-processed ZnO UV photodetector is employed in this work. It shows how electrons are injected into the ZnO nanoparticles from the electrode. Electron transport through hopping between particles is shown in the inset.

3. Results and Discussion
3.1. Surface Morphology
3.1.1 ZnO NPs Processed in Air

Figure 2- A and B shows the surface topography of ZnO films baked (annealing at low temperature for a few minutes) and annealed (treated at a relatively high temperature for a longer time) in air, respectively. AFM images illustrate the porous nature of ZnO NPs films prepared (spin coated and baked) and annealed in the atmosphere. ZnO NPs deposited in the air followed by soft baking at 100 ^{o}C for 10 min resulted in grain-like features spreading almost uniformly all over the surface, regardless of particle size, as illustrated in Figure 2-A. Surface roughness, taken from the full-size AFM image and depicts the surface imperfections, is 8 nm.
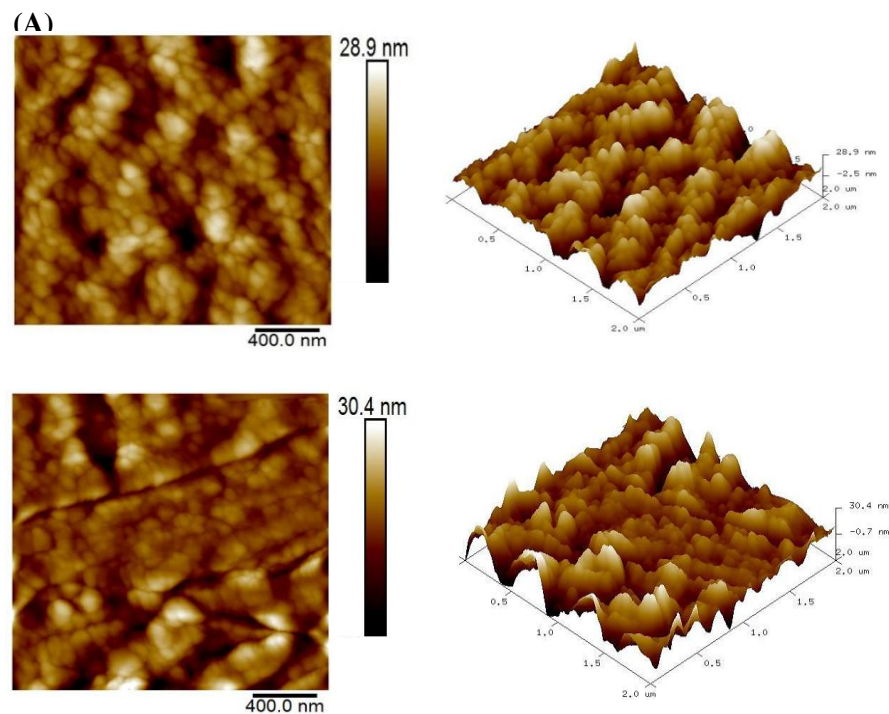

Figure 2: AFM images of ZnO nanoparticles deposited in air and processed at (A) 100°C for 10 min and (B) 350°C for 1h after baking. Surface roughness is calculated to be 8 nm for both films.

The AFM topography images of the ZnO nanoparticles prepared and annealed at 350 $^{\circ}$C in the air for 1 hour are shown in Figure 2-B. The two processing conditions, baking, and annealing have comparable surface morphology with a surface roughness of 8 nm.

3.1.2. ZnO NPs Processed in Nitrogen

Figure 3-A shows ZnO NPs films baked at 100 $^{\circ}$C for 10 minutes in the glove box (nitrogen environment). The film exhibits particle-like formations with larger agglomeration characteristics. The film's surface roughness is 8 nm, similar to the sample fabricated in the air. Surface morphology shows particle aggregation and surface roughness of 15 nm after 1 hour of annealing in nitrogen at 350°C as shown in Figure 3-B.
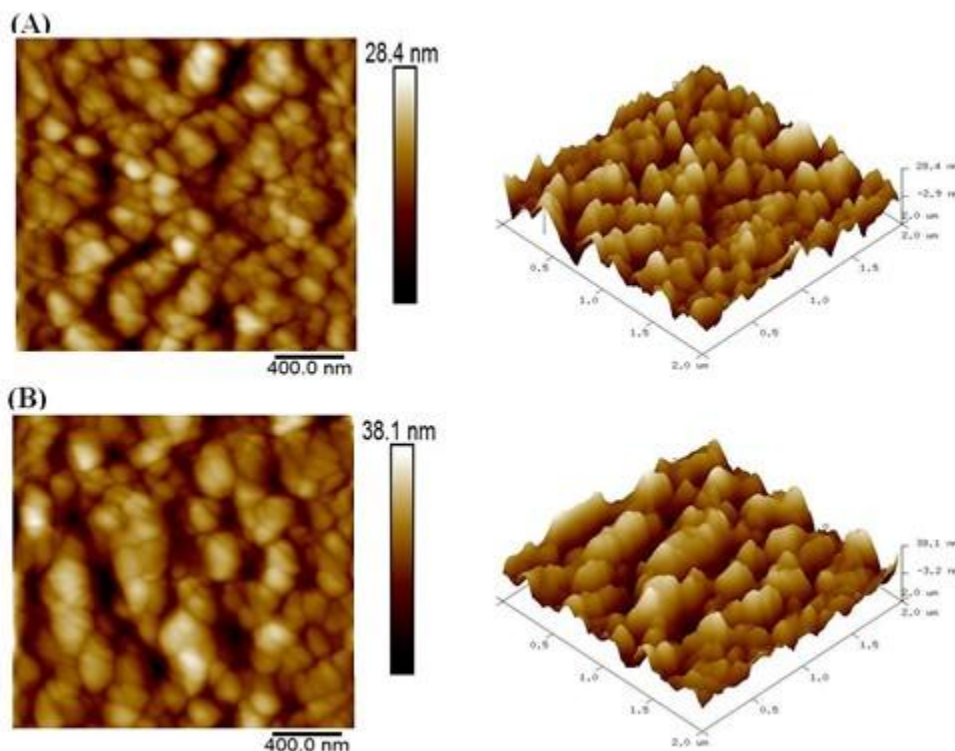

Figure 3: Surface topography of ZnO NP films prepared in the glove box surface processed at (A) 100°C for 10 min, surface roughness is 8 nm, and (B) 350°C for 1h, surface roughness is 15 nm.

3.2. FTIR Analysis of ZnO NPs

The effect of atmospheric conditions represented by atmospheric water and carbon species on the ZnO NPs surface was investigated by FTIR. ZnO nanoparticle films were deposited on GaAs substrates and studied using Fourier transform infrared spectroscopy. Figure 4 shows a comparison of FTIR spectra of ZnO NPs films before and after adding the organic capping ligands (octylamine) (these organic ligands help ZnO NPs to fully dissolve in organic solvents for better film quality) and also the FTIR spectrum of octylamine ligands alone. The figure shows the principal transition peaks, which provide an essential indicator of the influence of surface composition under different processing conditions. The transmission peak at around 500 cm^{-1} is given to the ZnO backbone transition. In comparison, the peak at 891 cm^{-1} is assigned to the hydrogen at the oxygen site (H$_O$) coupled to the lattice zinc site (Zn-HO) in the ZnO NPs film resulting from the zinc acetate precursor [19],[20], which behave as a shallow donor in ZnO [20]. Stretching bounds C=O and C-O are connected with the complex acetate (CH$_3$COO$^-$) groups chelated on the ZnO surface [21],[22],[23]. The poorly resolved doublet at 1415 and 1441 cm^{-1} are related to the weakly bonded water [22],[24] and also have been attributed to the asymmetrical and symmetrical stretching of zinc carboxylate [25],[23]. The FTIR spectra of the octylamine ligands (blue line) deposited on the GaAs substrate are shown in Figure 4-B. The FTIR of ZnO NPs film after adding the capping ligands of octylamine (red line) is shown in Figure 4-C. ZnO NPs films, before and after adding the ligands, show peaks at 2854 cm^{-1}, 2923 cm^{-1}, and 2956 cm^{-1}, assigned to symmetric and asymmetric C-H stretching in hydrocarbon chains [23],[26],[27].
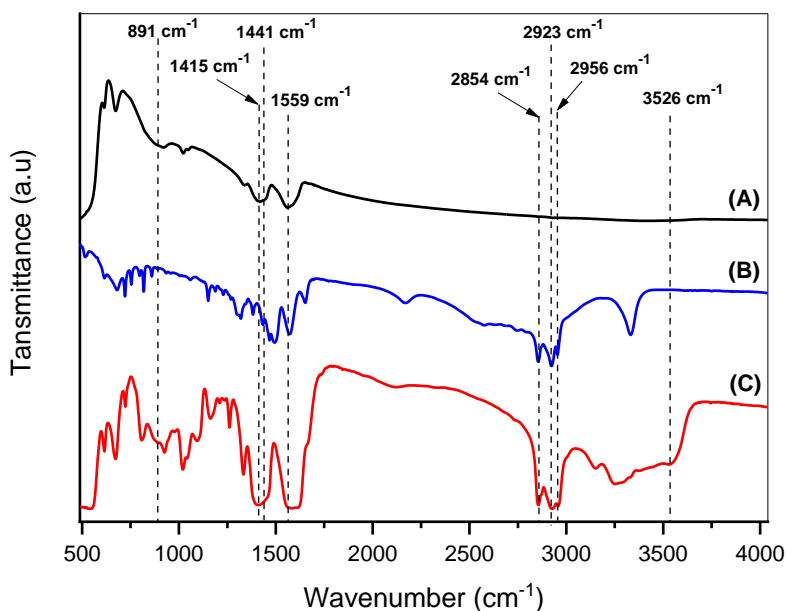
Figure 4: FTIR spectra of (A) ZnO film synthesized from zinc acetate precursor, (B) octylamine ligands with no treatment, (C) ZnO film showing in (A) after adding the octylamine ligands. Samples were deposited on GaAs substrates.

Figure 5 depicts the chemical composition of ZnO NPs films as a function of processing conditions, as revealed by FTIR spectra. The baked sample is used as a reference. It displays a vast number of transitions, most of which originate from the initial precursor's unbounded carbons and/or acetate groups. The reference ZnO NPs film (red line) utilized in this experiment was rather thick, which explains why some of the surface carbonate stretching vibrations were saturated. In comparison to the reference sample, several of the transition peaks are slightly displaced and the FTIR spectra become smoother when ZnO films are annealed at 350^oC for 1 hour in air and nitrogen, owing to the decomposition of most of the remaining carbons and unreacted chemical groups. When the ZnO NPs film is annealed in the air instead of nitrogen, the typical peaks at 1570 cm^{-1}, 1415 cm^{-1}, and 1450 cm^{-1} are ascribed to acetate groups from the starting precursor significantly reduced. In the latter condition, this shows that its breakdown is uncompleted. Figure 5 demonstrates a semi-complete degradation of the ligands connected to the ZnO NPs when preparing and annealing them in an oxidizing environment, as well as a greater relative absorption of water. The adsorbed carboxylate group on the surface (COO$^-$) [28] shows a peak at 1260 cm$^{-1,}$ which displays more substantial peaks in nitrogen and shifts to 1267 cm^{-1} after annealing. The octylamine ligands peaks are considerably reduced or eliminated after annealing in air and nitrogen, with just a tiny peak at 2956 cm^{-1} remaining, while the other two peaks at 2854 and 2923 cm^{-1} are essentially obliterated. The C-H bending modes of surface hydrocarbons [29] and carbonate ions CO_3^{2-} stretching mode [24] are thought to be ascribed to the two transition peaks situated approximately 806 cm^{-1} and 1020 cm^{-1} in the FTIR spectrum of the ZnO NPs film prepared and annealed in nitrogen, respectively. The two transition peaks are completely eliminated when ZnO NPs are prepared and annealed in air, as seen in the purple spectrum in Figure 5. Adsorbed water, which displays significant absorption after annealing in air, has a prominent absorption peak between 3000 and 3650 cm^{-1}.
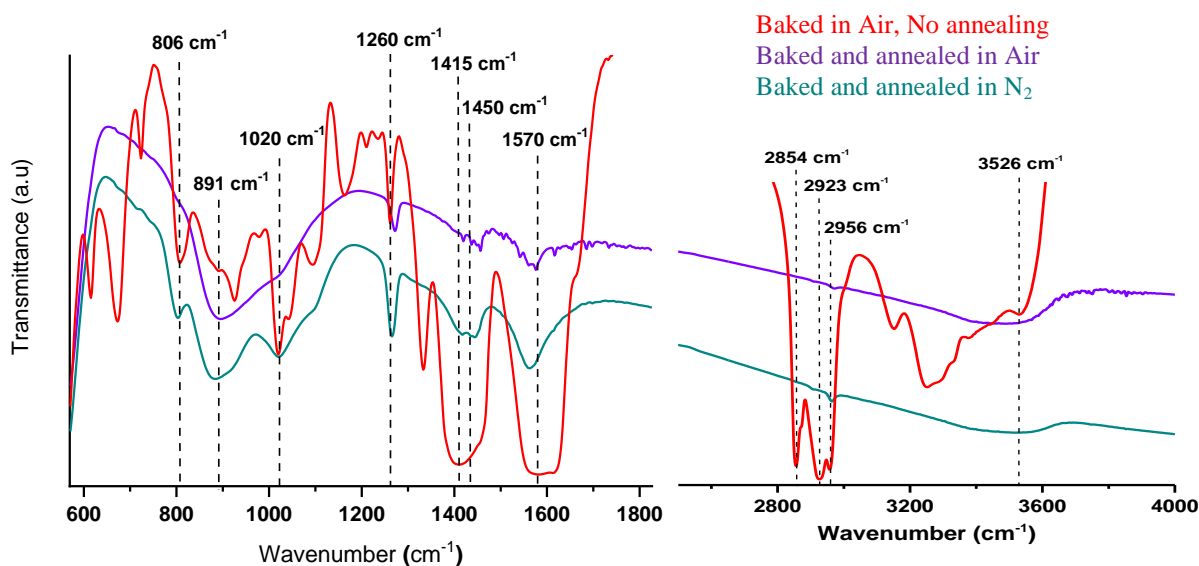
Figure 5: FTIR of ZnO nanoparticles films deposited on GaAs substrate after various processing conditions: Baked (soft annealing process) at 100 °C for 10 m in the air, baked and annealed at 350 °C for 1 hour in the air, and finally baked and annealed at 350 °C for 1 hour in nitrogen (glove box).

3.3. Photoconductivity of ZnO NPs

The photoconductivity of metal-semiconductor-metal (MSM) based on solution-processed ZnO NPs with planar device configuration was studied to determine what causes the persistent photoconductivity and what variables influence its magnitude. In the dark and after UV irradiation, we measured I-V properties, as well as the photocurrent spectrum and transients. To see if these parameters influenced photocurrent production, we evaluated ZnO NP devices made in air and nitrogen and tested them in various controlled atmospheres. The UV photoresponse of ZnO is thought to be affected by the adsorption of oxygen molecules from the ambient environment. Air combines water and carbon dioxide molecules, which may alter photocurrent production. We demonstrate that various surface species, such as water and/or surface carbonates, are equally important. Figure 6 displays the I-V characteristics of ZnO devices fabricated (spin-coated, baked, and annealed) in air and nitrogen, as well as photocurrent transients. The device prepared in the air (spin-coated and baked at 100°C for 10 min) acts as a reference device to the other two ZnO NP devices fabricated in air and nitrogen (prepared and annealed at 350°C for 1h). In the dark, ZnO NPs produced in the air exhibit asymmetric I-V behaviour, indicating charging effects. The dark current density was about 4.77×10^{-6} A/cm^2 at a voltage bias of 20 V. The device also exhibits asymmetric I-V behaviour when ZnO NPs are produced in air, with a dark current density of 4.27×10^{-7} A/cm^2 at 20 V. Figure 6-A shows that ZnO NPs manufactured in nitrogen had the lowest dark current, with a current density of 5.27×10^{-9} A/cm^2 at 20 V. The I-V characteristics of the devices were also tested in the presence of UV light with a wavelength of 363 nm and an intensity of 0.31 mW/cm^2 in the air. The sample fabricated in the air had the maximum photocurrent density, followed by the sample fabricated in nitrogen, and lastly the reference device, with responsivities of 11. 3, 1. 77, and 0. 23 A/W, respectively. When exposed to UV light, all three devices exhibit consistent and repeatable photocurrent cycles. Figure 6-B illustrates the temporal response of the devices by lighting the data at 1-minute intervals separated by 1minute gaps. The ZnO NPs device prepared in the air shows the lowest photocurrent of 7. 07×10^{-5} A/cm^2, compared to the device fabricated in the air which shows a photocurrent density of 9. 7×10^{-3} A/cm^2. Finally, the device fabricated in nitrogen shows a photocurrent density five orders of magnitudes higher than its dark current density, of 5.15×10^{-4} A/cm^2. However, these findings contradict those of Hatch et al. [27], which reported that photodetectors of ZnO-nanorod/CuSCN annealed in nitrogen had the maximum photocurrent in the UV, about 30 μA, when compared to oxygen and the air annealed samples. This is due to shallow N-related donor defects that arise during the strongly reducing nitrogen-anneal, as well as the lack of V_{Zn}^{2-} trap states. Figure 6- C to E shows photocurrent transients with slow reaction times, indicating persistent photoconductivity. As a result, the process of carriers being scavenged by adsorbed groups and forming volatile molecules that escape from the surface may be ruled

out. Water dissociation on the surface of ZnO has been observed to trap charge carriers and hence limit photocurrent [28]. However, in the second pulse, the current would be restored, which is not the case. Instead, the photo-decomposition of adsorbed moieties leads to the formation of long-lived defects on the surface that operate as recombination centres quenching carriers produced by future light pulses, as observed by the FTIR.
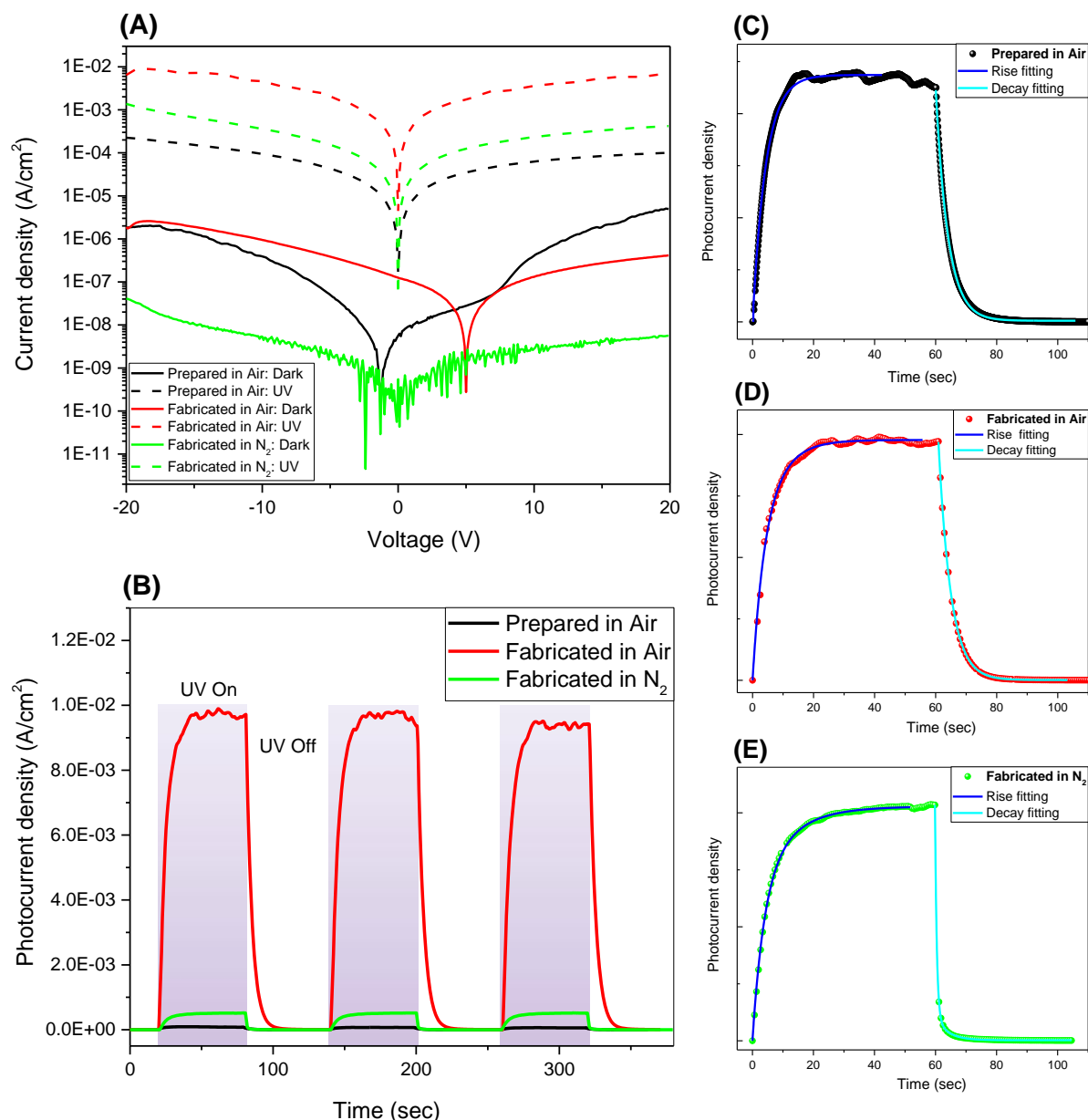

Figure 6: (A) I-V characteristics of ZnO NP films processed in nitrogen and air. (B) Photocurrent transients of the ZnO films. The devices were tested in the air at a voltage bias of 20 V. The photocurrent transients for devices processed in air and nitrogen are shown in (C), (D), and (E).

4. Conclusions

The effect of different atmospheric conditions on the UV photoconductivity of solution-processed ZnO NPs, such as atmospheric water and carbon species, has been studied. To do so, ZnO NPs films were spin-coated, baked at 100°C for 10 min and then annealed at 350°C for 1 hour (fabricated) in both air and inside the glove box (nitrogen environment). A detailed investigation of the origin of surface bonds located on the ZnO and its

relation to the processing environment is performed by FTIR spectroscopy analysis. ZnO photoconductivity is highly affected by the atmospheric adsorbed CO_2 from the air, which forms the carbonate groups on the ZnO surface. These groups passivate the surface states, leading to the release of trapped electrons and increasing the photoconductivity. ZnO films annealed in a nitrogen environment (no oxygen and water) retain a significant fraction of the starting precursor and ligands groups. Therefore, they show different photoconductivity behaviour than the films processed in the air.

Conflict of Interest: The authors declare that they have no conflict of interest.

References
[1] Y.-H. Zhang, Z.-X. Mei, H.-L. Liang, and X.-L. Du, "Review of flexible and transparent thin-film transistors based on zinc oxide and related materials," *Chinese Phys. B*, vol. 26, no. 4, p. 047307, Apr. 2017.
[2] C. L. Hsu, Y. H. Lin, L. K. Wang, T. J. Hsueh, S. P. Chang, and S. J. Chang, "Tunable UV- and Visible-Light Photoresponse Based on p-ZnO Nanostructures/n-ZnO/Glass Peppered with Au Nanoparticles," *ACS Appl. Mater. Interfaces*, vol. 9, no. 17, pp. 14935–14944, 2017.
[3] M. R. Alenezi, S. J. Henley, and S. R. P. Silva, "On-chip fabrication of high performance nanostructured ZnO UV detectors.," *Sci. Rep.*, vol. 5, p. 8516, 2015.
[4] S. Khudiar, U. Nayef, and F. Mutlak, "Preparation and Characterization of Porous Silicon for Photodetector Applications," *J. Appl. Sci. Nanotechnol.*, vol. 2, no. 2, pp. 64–69, Jun. 2022.
[5] R. Saleh, O. Salman, and M. Dawood, "Physical Investigations of Titanium Dioxide Nanorods Film Prepared by Hydrothermal Technique," *J. Appl. Sci. Nanotechnol.*, vol. 1, no. 3, pp. 32–41, Oct. 2021.
[6] A. Thajeel, M. Ibrahem, and D. Ahmed, "Nanoplasmonic Sensing Using Gold Nanostructures," *J. Appl. Sci. Nanotechnol.*, vol. 2, no. 2, pp. 8–15, Jun. 2022.
[7] Y. Y. Lin, C. C. Hsu, M. H. Tseng, J. J. Shyue, and F. Y. Tsai, "Stable and High-Performance Flexible ZnO Thin-Film Transistors by Atomic Layer Deposition," *ACS Appl. Mater. Interfaces*, vol. 7, no. 40, pp. 22610–22617, 2015.
[8] B. H. Kind, H. Yan, B. Messer, M. Law, and P. Yang, "Nanowire Ultraviolet Photodetectors and Optical Switches," *Adv. Mater.*, vol. 14, no. 2, pp. 158–160, 2002.
[9] C. Soci *et al.*, "ZnO Nanowire UV Photodetectors with High Internal Gain," *Nano Lett.*, vol. 7, no. 4, pp. 1003–1009, Apr. 2007.
[10] A. Bera and D. Basak, "Role of defects in the anomalous photoconductivity in ZnO nanowires," *Appl. Phys. Lett.*, vol. 94, no. 16, p. 163119, Apr. 2009.
[11] R. J. Collins and D. G. Thomas, "Photoconduction and surface effects with zinc oxide crystals," *Phys. Rev.*, vol. 112, no. 2, pp. 388–395, 1958.
[12] J. Bao *et al.*, "Photoinduced oxygen release and persistent photoconductivity in ZnO nanowires.," *Nanoscale Res. Lett.*, vol. 6, no. 1, p. 404, 2011.
[13] R. Gurwitz, R. Cohen, and I. Shalish, "Interaction of light with the ZnO surface: Photon induced oxygen 'breathing,' oxygen vacancies, persistent photoconductivity, and persistent photovoltage," *J. Appl. Phys.*, vol. 115, no. 3, 2014.
[14] M. A. Ibrahem *et al.*, "Dual Wavelength (Ultraviolet and Green) Photodetectors Using Solution Processed Zinc Oxide Nanoparticles," *ACS Appl. Mater. Interfaces*, vol. 9, no. 42, pp. 36971–36979, Oct. 2017.
[15] H. Zhang, Y. Hu, Z. Wang, Z. Fang, and L. M. Peng, "Performance Boosting of Flexible ZnO UV Sensors with Rational Designed Absorbing Antireflection Layer and Humectant Encapsulation," *ACS Appl. Mater. Interfaces*, vol. 8, no. 1, pp. 381–389, 2016.
[16] S. Chatman and K. M. Poduska, "The Effect of Synthesis Conditions and Humidity on Current−Voltage Relations in Electrodeposited ZnO-Based Schottky Junctions," *ACS Appl. Mater. Interfaces*, vol. 1, no. 3, pp. 552–558, Mar. 2009.
[17] Y. Jin, J. Wang, B. Sun, J. C. Blakesley, and N. C. Greenham, "Solution-Processed Ultraviolet Photodetectors Based on Colloidal ZnO Nanoparticles," *Nano Lett.*, vol. 8, no. 6, pp. 1649–1653, Jun. 2008.
[18] M. A. Ibrahem, E. Verrelli, F. Cheng, A. M. Adawi, J.-S. G. Bouillard, and M. O'Neill, "Persistent near-infrared photoconductivity of ZnO nanoparticles based on plasmonic hot charge carriers," *J. Appl. Phys.*,

vol. 131, no. 10, p. 103103, Mar. 2022.

[19]   R. Kumari, A. Sahai, and N. Goswami, "Effect of nitrogen doping on structural and optical properties of ZnO nanoparticles," *Prog. Nat. Sci. Mater. Int.*, vol. 25, no. 4, pp. 300–309, 2015.

[20]   K. Senthilkumar, M. Tokunaga, H. Okamoto, O. Senthilkumar, and Y. Fujita, "Hydrogen related defect complexes in ZnO nanoparticles," *Appl. Phys. Lett.*, vol. 97, no. 9, p. 091907, Aug. 2010.

[21]   J. H. Taylor and C. H. Amberg, "Infrared spectra of gases chemisorbed on zinc oxide: CO and CO2," *Can. J. Chem.*, vol. 39, no. 3, pp. 535–539, Mar. 1961.

[22]   S. Sakohara, L. D. Tickanen, and M. A. Anderson, "Luminescence Properties of Thin Zinc Oxide Membranes Prepared by the Sol-Gel Technique: Change in Visible Luminescence during Flring," *J. Phys. Chem*, vol. 96, pp. 11086–11091, 1992.

[23]   K. Yadav, B. R. Mehta, S. Bhattacharya, and J. P. Singh, "A fast and effective approach for reversible wetting-dewetting transitions on ZnO nanowires," *Sci. Rep.*, vol. 6, no. 1, p. 35073, Dec. 2016.

[24]   Z. Lin, F. Guo, C. Wang, X. Wang, K. Wang, and Y. Qu, "Preparation and sensing properties of hierarchical 3D assembled porous ZnO from zinc hydroxide carbonate," *RSC Adv.*, vol. 4, no. 10, p. 5122, 2014.

[25]   G. Xiong, U. Pal, J. G. Serrano, K. B. Ucer, and R. T. Williams, "Photoluminesence and FTIR study of ZnO nanoparticles: the impurity and defect perspective," *Phys. status solidi*, vol. 3, no. 10, pp. 3577–3581, Nov. 2006.

[26]   T. Cun, C. Dong, and Q. Huang, "Ionothermal precipitation of highly dispersive ZnO nanoparticles with improved photocatalytic performance," *Appl. Surf. Sci.*, vol. 384, pp. 73–82, 2016.

[27]   S. Kumar and P. D. Sahare, "Effect of surface defects on green luminescence from ZnO nanoparticles," *AIP Conference Proceedings*, vol. 1393. pp. 159–160, 2011.

[28]   J. Saussey, J.-C. Lavalley, and C. Bovet, "Infrared study of CO2 adsorption on ZnO. Adsorption sites," *J. Chem. Soc. Faraday Trans. 1 Phys. Chem. Condens. Phases*, vol. 78, no. 5, p. 1457, 1982.

[29]   Andreas J. Nuber, "Reversible wettability of nanoscale ZnO arrays," University of New Jersey.